Am J Physiol Cell Physiol 305: C1060–C1068, 2013.
First published September 4, 2013; doi:10.1152/ajpcell.00077.2013.

Extracellular Ca^{2+} and Mg^{2+} modulate aminoglycoside blockade of mechanotransducer channel-mediated Ca^{2+} entry in zebrafish hair cells: an in vivo study with the SIET

Li-Yih Lin,[1] Wei Pang,[1] Wei-Min Chuang,[1] Giun-Yi Hung,[2,3] Yuan-Hsiang Lin,[4] and Jiun-Lin Horng[5]

[1]*Department of Life Science, National Taiwan Normal University, Taipei, Taiwan, Republic of China;* [2]*Department of Pediatrics, Taipei Veterans General Hospital, Taipei, Taiwan, Republic of China;* [3]*Department of Pediatrics, Faculty of Medicine, National Yang-Ming University, Taipei, Taiwan, Republic of China;* [4]*Department of Electronic Engineering, National Taiwan University of Science and Technology, Taipei, Taiwan, Republic of China; and* [5]*Department of Anatomy, Taipei Medical University, Taipei, Taiwan, Republic of China*

Submitted 19 March 2013; accepted in final form 28 August 2013

Lin LY, Pang W, Chuang WM, Hung GY, Lin YH, Horng JL. Extracellular Ca^{2+} and Mg^{2+} modulate aminoglycoside blockade of mechanotransducer channel-mediated Ca^{2+} entry in zebrafish hair cells: an in vivo study with the SIET. *Am J Physiol Cell Physiol* 305: C1060–C1068, 2013. First published September 4, 2013; doi:10.1152/ajpcell.00077.2013.—Zebrafish lateral-line hair cells are an in vivo model for studying hair cell development, function, and ototoxicity. However, the molecular identification and properties of the mechanotransducer (MET) channel in hair cells are still controversial. In this study, a noninvasive electrophysiological method, the scanning ion-electrode technique (SIET), was applied for the first time to investigate properties of MET channels in intact zebrafish embryos. With the use of a Ca^{2+}-selective microelectrode to deflect hair bundles and simultaneously record the Ca^{2+} flux, the inward Ca^{2+} flux was detected at stereocilia of hair cells in 2- to ~4-day postfertilization embryos. Ca^{2+} influx was blocked by MET channel blockers (BAPTA, La^{3+}, Gd^{3+}, and curare). In addition, 10 μM aminoglycoside antibiotics (neomycin and gentamicin) were found to effectively block Ca^{2+} influx within 10 min. Elevating the external Ca^{2+} level (0.2–2 mM) neutralized the effects of neomycin and gentamicin. However, elevating the Mg^{2+} level up to 5 mM neutralized blockade by gentamicin but not by neomycin. This study demonstrated MET channel-mediated Ca^{2+} entry at hair cells and showed that the SIET to be a sensitive approach for functionally assaying MET channels in zebrafish.

aminoglycoside; hair cell; MET channel; neuromast; SIET

OTOTOXINS ARE COMPOUNDS KNOWN to cause damage to the hearing and balance systems of animals. It was reported that >130 common medicines are ototoxic including aminoglycosides (AGs), antimalarials, salicylates, loop diuretics, and antineoplastic agents (52). Among these ototoxins, AGs are well-known and commonly used antibiotics such as streptomycin, dihydrostreptomycin (DHS), neomycin, tobramycin, kanamycin, paromomycin, spectinomycin, gentamicin, netilmicin, and amikacin (27). In general, AGs cause hair cell damage or even death in cochlear and/or vestibular organs. Despite this, AGs are still the most commonly prescribed antibiotics, and currently there is no standard treatment for drug-induced ototoxicity (27).

Studies in rats and humans showed that AGs enter perilymph and endolymph fluids shortly after injection into the bloodstream, but the concentration in the inner ear never exceeds the level in plasma (3, 59). Although they are removed from the blood within hours, AGs can remain within cells of the inner ear for many months (15). In the prevailing model, AGs in the endolymph are taken up by hair cells through the mechanotransducer (MET) channel (1, 36, 61). Entry of AGs into hair cells is thought to trigger formation of reactive oxygen species and activation of caspase signaling and ultimately lead to cell apoptosis (62).

MET channels are located at the tips of actin-filled stereocilia (hair bundles) of hair cells and are gated by an elastic element, the "tip link," connecting stereocilia and kinocilia (18, 19, 44, 51). Sound-induced deflection of a hair bundle in the direction of the longest stereocilia stretches the tip link, thus opening the MET channel and initiating mechanotransduction (18, 19, 51). In the vertebrate inner ear, hair bundles are bathed in endolymph in which resides high K^+, and mechanotransduction is predominantly activated by K^+ entry through MET channels (18, 65). However, electrophysiological analysis of isolated hair cells showed that MET channel is a nonselective cation channel with high Ca^{2+} permeability, which passes Ca^{2+} at least fives times better than it does Na^+ and K^+ (18). In addition, MET channels were also found to pass small organic molecules such as the fluorescent styryl dye FM1–43, which is used as a marker of hair cell viability and functionality (16, 21, 38, 43).

Several studies suggested that functioning of MET channels is important for AG ototoxicity. For example, both noise exposure and acoustic stimuli were found to increase the probability that MET channels were open, thereby increasing ototoxic damage by AGs (27, 33). In the mouse cochlea and zebrafish lateral line, high levels of extracellular Ca^{2+} or Mg^{2+} can protect hair cells from neomycin- and gentamicin-induced cell death, suggesting that high Ca^{2+} levels reduce AG uptake through MET channels of hair cells (8, 49, 61). In contrast, lowering extracellular Ca^{2+} increased the probability that MET channels are open (11, 17, 47, 48), amplified the blocking efficacy of DHS (46), and increased AG toxicity toward hair cells (8). Moreover, AGs were reported to block MET ion currents as they pass through MET channels (32, 41, 44, 46) and accumulated rapidly within hair cells (36, 60).

Functional studies of inner ear hair cells of mammals, birds, and other vertebrates are limited by the difficulty in accessing the inner ear, which is embedded in the temporal bone. Moreover, with the systemic administration of AGs, it is difficult to determine the dose of the drug that reaches hair cells. Zebrafish

Address for reprint requests and other correspondence: J.-L. Horng, Dept. of Anatomy, Taipei Medical Univ., Taipei, Taiwan 110, ROC (e-mail: jlhorng@tmu.edu.tw).

were recently reported to be a useful in vivo model for studying hair cells and ototoxicity (7, 20, 43, 58). Hair cells of zebrafish are organized into lateral line neuromasts on the embryonic skin and can be easily observed and investigated (23, 29, 45). Neuromasts on the head form the anterior lateral line (ALL) system, which comprises the otic line (OT), supraorbital line (SO), middle line (MI), occipital line (OC), infraorbital line (IO), mandibular line (MD), and opercular line (OP) (23, 29, 45), while neuromasts on the body and tail form the posterior lateral line (PLL) system, which comprises five regularly spaced neuromasts (L1~L5) along each flank and two or three terminal neuromasts at the tip of the tail (23, 29, 45). The structure and function of lateral-line hair cells are similar to those of inner-ear hair cells in other vertebrates including humans, and lateral-line hair cells are also sensitive to ototoxic drugs including AGs and cisplatin (7, 20, 42, 43, 58). These properties make the zebrafish an ideal model for ototoxic drug screening.

In the present study, a noninvasive electrophysiological scanning ion-electrode technique (SIET) was applied to analyze MET channel-mediated Ca^{2+} influx (56) in lateral-line hair cells of intact zebrafish embryos. With this technique in zebrafish, we attempted to establish a new, powerful approach to functionally study vertebrate hair cells and MET channels. The SIET has been instrumental in detecting very weak ion fluxes near cells and tissues that arise as ions cross cell membranes through ion channels or transporters. It was used to detect H^+, K^+, NH_4^+, Na^+, and Cl^- gradients adjacent to anal papillae, the ion regulatory organ of mosquito larvae (13, 14). It was also used to respectively measure H^+, Cl^-, and Ca^{2+} fluxes near retina cells (31), kidney cell lines (22), and mouse blastocysts (56). In plant tissues, the SIET was used to measure H^+, Na^+, and Cl^- fluxes in roots and pollen tubes (37, 57). In our previous studies, we applied the SIET to study Na^+, Cl^-, NH_4^+, and H^+ transport by ionocytes in the embryonic skin of zebrafish and medaka (25, 26, 28, 34, 53–55, 64). The SIET uses a motion-controlled oscillating ion-selective microelectrode to measure ionic gradients between two spatial points (usually <10 μm apart) at the surface of target cells, and the ionic gradients can be converted to ionic fluxes between the two points. In this study, we used an oscillating Ca^{2+}-selective microelectrode to deflect the kinocilia of hair cells and simultaneously record Ca^{2+} fluxes at the apical surfaces of neuromasts. We successfully measured MET channel-mediated Ca^{2+} influxes at stereocilia and found that the Ca^{2+} influx was blocked by MET channel inhibitors (La^{3+}, Gd^{3+}, BAPTA, and curare) and AGs (neomycin and gentamycin). We also showed that Ca^{2+} and Mg^{2+} can protect MET channels from AG blockade with different potencies.

MATERIALS AND METHODS

Zebrafish. Adult zebrafish (AB strain) were reared in circulating tap water at 28°C with a photoperiod of 14 h of light/10 h of dark. Fertilized eggs were incubated in artificial normal water (NW). The NW contained the following (in mM): 0.5 NaCl, 0.2 $CaSO_4$, 0.2 $MgSO_4$, 0.16 KH_2PO_4, and 0.16 K_2HPO_4 (pH 7.0). All of the incubating solutions were prepared by addition of various salts (Sigma-Aldrich, St. Louis, MO) to double-distilled water. During the experiments, embryos were not fed, and the NW was changed daily to ensure optimal water quality. The experimental protocols were approved by the Taipei Medical University Animal Care and Utilization Committee (Approval No. LAC-99-0160).

Ion-selective microelectrodes. To construct ion-selective microelectrodes, glass capillary tubes (no. TW 150-4; World Precision Instruments, Sarasota, FL) were pulled on a Sutter P-97 Flaming Brown pipette puller (Sutter Instruments, San Rafael, CA) into micropipettes with tip diameters of 3~4 μm. The micropipettes were then baked at 120°C overnight and coated with dimethyl chlorosilane (Sigma-Aldrich) for 30 min. The micropipettes were backfilled with a 1-cm column of 100 mM $CaCl_2$ (or KCl; Sigma-Aldrich) for the Ca^{2+}-selective microelectrode (or K^+-selective microelectrode). The microelectrode was then frontloaded with a 20- to ~30-μm column of Ca^{2+} ionophore I cocktail A (or 100 μm of K^+ ionophore I cocktail A; Sigma-Aldrich) to create a Ca^{2+}-selective microelectrode (or K^+-selective microelectrode).

SIET. Details of the system were described in previous reports (24, 54, 64). Briefly, the ion-selective microelectrode was connected to the main amplifier via an Ag/AgCl wire electrode holder and preamplifier (Fig. 1*A*; Applicable Electronics, East Falmouth, MA), and the circuit was completed with a salt bridge (3 M KCl in 3% agarose connected to an Ag/AgCl wire). Oscillation and positioning of the microelectrode were performed with a step-wise motor-driven three-dimensional (3D) positioner (Applicable Electronics) that was attached to an Olympus upright microscope (Fig. 1*A*; BX-50WI; Olympus, Tokyo, Japan). A ×10 dry lens and ×60 water-immersion objective lens were used for observations. The microscope was equipped with a digital camera (EOS 50D; Canon, Tokyo, Japan) that allowed images to be visualized on a monitor and recorded. Data acquisition, preliminary processing, and control of the 3D electrode positioner were performed with ASET software (Science Wares, East Falmouth, MA).

Calibration of ion-selective microelectrodes. To calibrate the ion-selective microelectrodes, the Nernstian property of each microelectrode was measured by placing the microelectrode in a series of standard solutions (Ca^{2+} microelectrode: 0.1, 1, 10, and 100 mM $CaCl_2$; K^+ microelectrode: 0.1, 1, 10, and 100 mM KCl). By plotting the voltage output of the probe against log [Ca^{2+}] and log [K^+] values, a linear regression yielded a Nernstian slope of 28.5 ± 0.4 ($n = 10$) for Ca^{2+} and 55.9 ± 0.6 ($n = 10$) for K^+. According to technical documents provided by Sigma, the selectivity coefficients of the Fluka Ca^{2+} ionophore I cocktail A is ~1,000 times more selective to Ca^{2+} than to Mg^{2+}.

Measurement of Ca^{2+} flux at neuromasts. The SIET (Fig. 1*A*) was performed at room temperature (26~28°C) in a small plastic recording chamber filled with 1 ml of recording medium that contained NW, 300 μM MOPS buffer, and 0.1 mg/l ethyl 3-aminobenzoate methanesulfonate (tricaine; Sigma-Aldrich). The pH of the recording medium was adjusted to 7.0 by adding a NaOH or HCl solution. Before being measured, an anesthetized embryo was positioned in the center of the chamber with its lateral side contacting the base of the chamber, and it was observed through a ×60 water-immersion lens. Then, the microelectrode was moved into the recording medium and positioned at the apical surface of a neuromast (X_0; Fig. 1, *B* and *C*) to record Ca^{2+} activity. The microelectrode oscillated between X_0 and X_1 at an interval of 10 μm. As the microelectrode moved from X_1 to X_0, it deflected kinocilia (*arrow K*) and led to opening of the MET channel on the stereocilia (Fig. 1*B*, *arrow S*). Figure 1*C* shows a microscopic image of the microelectrode at the apical surface of a neuromast with kinocilia extending from the apical surface. As the microelectrode oscillated, voltage differences (in microvolts) between X_0 and X_1 were recorded (Fig. 1*B*). The recordings were usually performed on a neuromast for 5~10 replicates, and the median value was used to calculate ionic fluxes between X_0 and X_1 with ASET software (Applicable Electronics). Briefly, voltage gradients obtained from the ASET software were converted into concentration (activity) gradients using the following equation: $\Delta C = C_b \times 10^{(\Delta V/S)} - C_b$, where ΔC is the concentration gradient between the two points measured in micromoles per liter per centimeters squared, C_b is the background ion

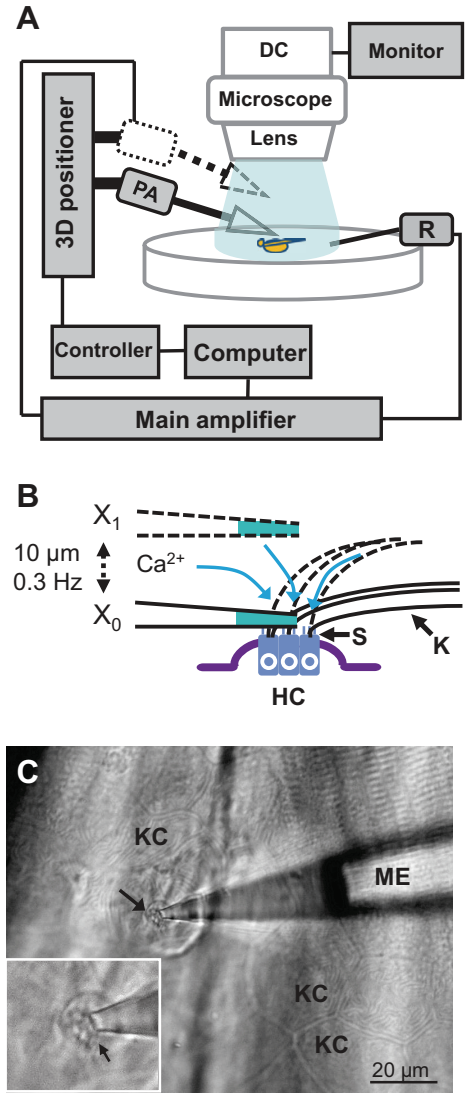

Fig. 1. Illustration of the scanning ion-electrode technique (SIET). *A*: an anesthetized embryo was positioned in a recording chamber filled with recording medium on the stage of an upright microscope equipped with a water-immersion lens. Microscopic image was obtained with a digital camera (DC) connected to a high-definition color monitor. The Ca^{2+}-selective microelectrode was mounted on a 3-dimensional microstepping motor positioner that was controlled by a computer via a controller. Voltage signals were amplified by a ×10 preamplifier (PA) followed by a ×100 main amplifier and were finally converted to digital signals for computer recording (R) and analysis. *B*: illustration of SIET probing of neuromast hair cells (HC). The Ca^{2+}-selective microelectrode was moved to the apical surface of a neuromast and oscillated (at 0.3 Hz) between 2 points (X_1 and X_0) at an interval of 10 μm. The X_0 position was about 1~2 μm above the apical surface of the neuromast (*arrow S*). As the electrode moved between X_1 and X_0, it deflected the kinocilia (*arrow K*), and voltage differences between the 2 points were recorded. *C*: microscopic image showed SIET probing of a neuromast. The Ca^{2+}-selective microelectrode (ME) was positioned at X_0. Arrows indicate kinocilia. KCs, keratinocytes.

concentration, calculated as the average of the concentration at each point measured in micromoles per liter, ΔV is the voltage gradient obtained from ASET in microvolts, and S is the Nernst slope of the electrode. The concentration gradient was subsequently converted into an (extracellular) ion flux using Fick's law of diffusion in the following equation: $J = D(\Delta C)/\Delta X$, where J is the net flux of the ion (in pmol·cm^{-2}·s^{-1}), D is the diffusion coefficient (of 8×10^{-6} cm^2·s^{-1} for Ca^{2+} and 2×10^{-5} cm^2·s^{-1} for K^+), ΔC is the concentration gradient (in pmol·cm^{-3}), and ΔX is the distance between the two points (in centimeters).

Drug preparation and treatment. BAPTA, La^{3+}, Gd^{3+}, and tubocurarine (curare) (Sigma-Aldrich) were, respectively, dissolved in NW to final concentrations of 10~5,000 μM. Neomycin (10 mg/ml; Sigma-Aldrich) and gentamicin (10 mg/ml, Sigma-Aldrich) were dissolved in NW to final concentrations of 1, 10, 100, and 1,000 μM (pH 7.0). To prepare NW with different Ca^{2+} levels, $CaSO_4$ was dissolved in NW to produce solutions of 0.5, 1, 1.5, and 2 mM. To prepare NW with different Mg^{2+} levels, $MgSO_4$ was dissolved in NW to produce solutions of 1, 2, 5, and 10 mM. Media were adjusted to pH 7.0. Before the SIET measurement, embryos were immersed in drug medium for 30 min. Thereafter, embryos were measured in recording medium without the drugs.

Statistical analysis. Data are expressed as the means ± SE. Values from each condition were analyzed using a one-way ANOVA followed by Tukey's pairwise comparisons. Student's unpaired *t*-test (two-tailed) was used for simple comparisons of 2 means. In all cases, significance was accepted at a level of 0.05.

RESULTS

Detection of Ca^{2+} flux in neuromasts of zebrafish embryos. To locate Ca^{2+} entry into a neuromast, the microelectrode was positioned at *locations 1*, *2*, and *3* to record Ca^{2+} fluxes on L1 neuromast of 4-day postfertilization (dpf) zebrafish embryos (Fig. 2*A*). The SIET detected the largest Ca^{2+} influxes (with negative values indicating an influx of cations) at *location 1* (Fig. 2*B*) and much smaller influxes and even effluxes at *locations 2* and *3* and the keratinocyte (KC in Fig. 2*B*), indicating that Ca^{2+} entry occurred right at the apical surface of hair cells where stereocilia are located. Therefore, MET channel-mediated ion fluxes were measured at *location 1* in the following experiments. No significant Ca^{2+} influx was detected when kinocilia were not deflected by the microelectrode (data not shown). Outward Ca^{2+} flux was found at keratinocytes covering the entire embryo indicating that body fluid Ca^{2+} passively diffuses out of embryonic skin (Fig. 2*B*). Similar NH_4^+, Na^+, and Cl^- outflows from the skin of fish embryos were also found in our previous studies (34, 53, 55, 64). Therefore, keratinocytes adjacent to neuromasts were measured as a negative control in this study.

To test if the addition of tricaine affected Ca^{2+} flux of neuromasts, a sequential recording on the same neuromast was conducted in an embryo before and after treatment with tricaine. Figure 2*C* shows the recorded voltage differences and fluxes at the background (5 mm away from the embryo) and at a neuromast in a 3-dpf embryo. The value of the neuromast was remarkably larger than that of the background. The addition of tricaine did not affect the Ca^{2+} influx at neuromasts (Fig. 2*D*). Therefore, tricaine was applied to embryos to prevent unnecessary movements by embryos in this study.

Because the MET channel mainly permeates K^+ in the inner ear (see DISCUSSION), we also used a K^+-selective microelectrode to detect K^+ fluxes at neuromasts. Moderate and comparable K^+ effluxes were detected at both hair cells and adjacent keratinocytes (Fig. 3*A*), indicating that K^+ efflux was not mediated by MET channels. Furthermore, the Ca^{2+} influx at neuromasts was not suppressed by a high external K^+ level (5 mM; Fig. 3*B*), suggesting that the MET channel is specific to Ca^{2+}.

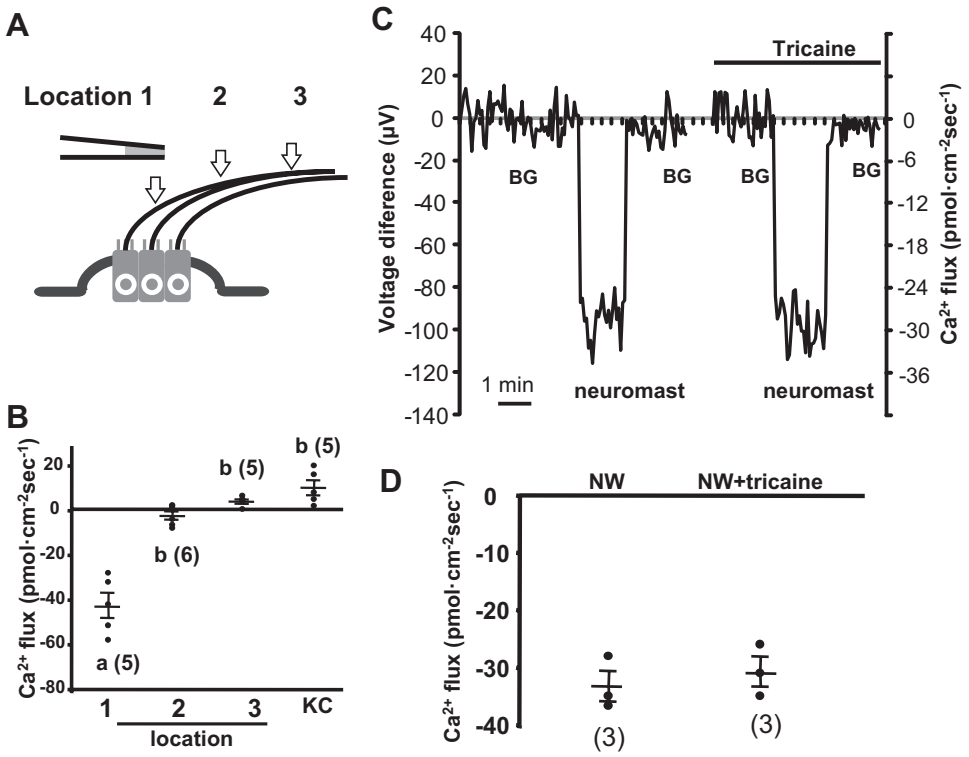

Fig. 2. Location of Ca^{2+} entry at a neuromast. *A*: illustration of SIET probing at different locations of a hair bundle. The microelectrode was moved to *locations 1* (apical surface of a neuromast), *2* (middle of the kinocilia), and *3* (tip of the kinocilia) to detect Ca^{2+} fluxes. *B*: Ca^{2+} influxes measured at the 3 locations and KC. *C*: raw data of neuromast Ca^{2+} influx detected by the SIET system, and the effect of an anesthetic (tricaine) is shown. BG, background. *D*: effect of tricaine on Ca^{2+} influx of HC. NW, normal water. Data are presented as the means ± SE. Numbers in parentheses are neuromast numbers. [a,b]Significant difference (by one-way ANOVA, Tukey's comparison, $P < 0.05$).

Blockade of the MET channel by BAPTA, La^{3+}, Gd^{3+}, and curare. BAPTA is used to break the tip links of hair cells and was found to abolish mechanotransduction in both nonmammals and mammals (2, 16, 46). La^{3+}, Gd^{3+}, and curare are also known to block MET channels in mammals (18). Herein, we used these drugs to verify that the Ca^{2+} influx of neuromasts was mediated by MET channels. Embryos were preincubated in NW with adequate drugs for 30 min and measured with SIET in recording medium without drugs. Figure 4 shows that BAPTA, La^{3+}, Gd^{3+}, and curare significantly inhibited Ca^{2+} influx with dose-dependent responses, supporting that the detected Ca^{2+} influx was mediated by MET channels.

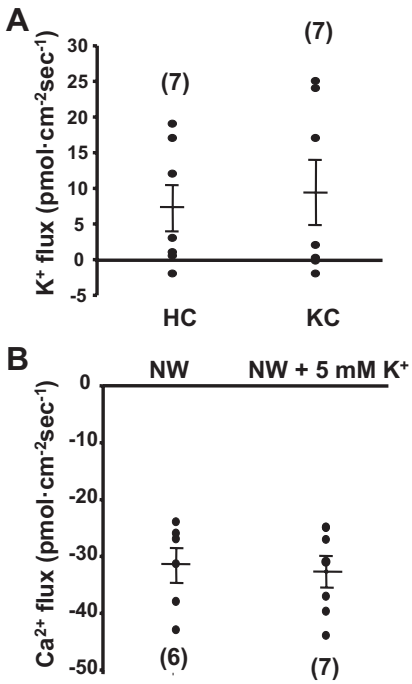

Fig. 3. Detection of K^+ flux and the effect of extracellular K^+ on the Ca^{2+} influx of HC. *A*: K^+ effluxes were detected at neuromast HC and KC. *B*: effect of high K^+ (5 mM) on the Ca^{2+} influx of HC. Data are presented as the means ± SE. Numbers in parentheses are neuromast numbers.

The MET channel mediates Ca^{2+} influx during embryonic development. To determine the onset of MET channels during zebrafish development, Ca^{2+} influxes of ALL (MI1) and PLL neuromasts (L1 and L3) (23, 29, 45) were measured in 2-, 3-, and 4-dpf embryos (Fig. 5). At 2 dpf, Ca^{2+} influx was detected at MI1 and L1 neuromasts but not at the L3 one (no hair bundle was found at L3). Ca^{2+} influx at L1 (MI1) at 2 dpf was significantly lower than that of L1 (MI1) at 3 dpf. At 3 and 4 dpf, no significant difference was found among MI1, L1, and L3 (Fig. 5), suggesting that hair-cell functions of MI1, L1, and L3 had matured by 3 dpf. In the following experiments, we measured L1, L2, and L3 neuromasts of 4-dpf embryos.

Inhibition of the Ca^{2+} influx of neuromasts by AGs. Various doses of neomycin and gentamicin were applied to examine the effects of AGs on Ca^{2+} influx of neuromasts. Real-time recordings of Ca^{2+} influxes in embryos treated with 10 μM neomycin/gentamicin are shown in Figs. 6, *A* and *D*. Ca^{2+} influx was detected before the addition of AGs, but the influx gradually declined after addition of AGs (arrows in Fig. 6, *A* and *D*). After 10 min, the Ca^{2+} influx was suppressed to a very low level. In the following AG experiments, embryos were preincubated in NW with adequate AGs for 30 min and measured by the SIET in recording medium without the AGs. Dose-dependent inhibition of Ca^{2+} influx was found in embryos treated with 1, 10, 100, and 1,000 μM AGs for 30 min (black dot in Fig. 6, *B* and *E*). Inhibition by AGs did not

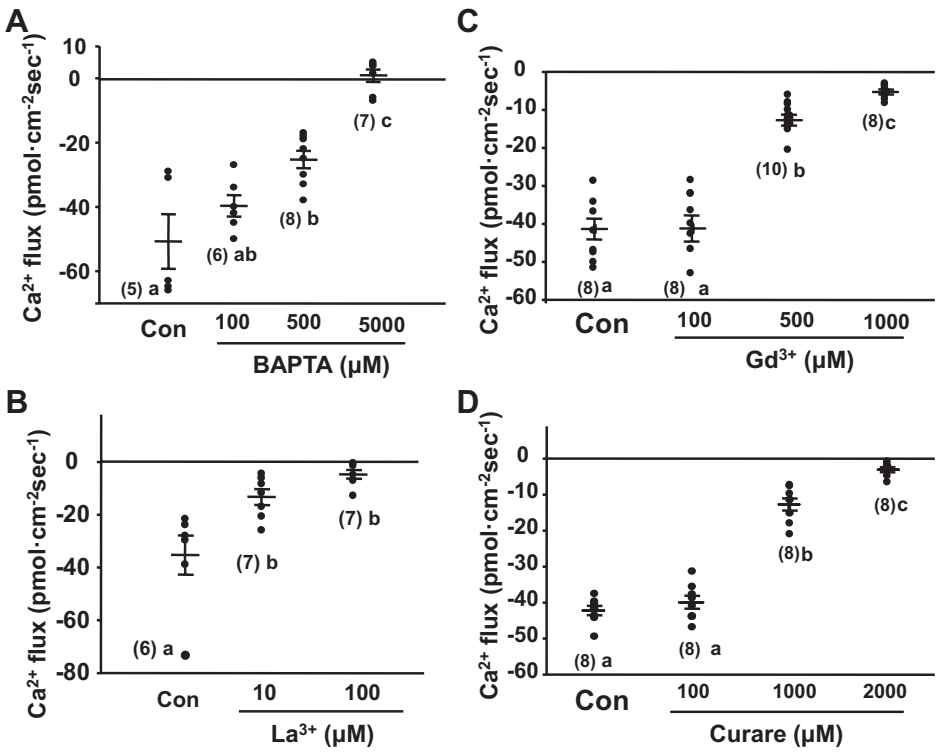

Fig. 4. Effects of BAPTA, La^{3+}, Gd^{3+}, and curare on Ca^{2+} influx of neuromasts. BAPTA (*A*), La^{3+} (*B*), Gd^{3+} (*C*), and curare (*D*) significantly blocked the Ca^{2+} influx of neuromast HC. Data are presented as the means ± SE. [a,b,c]Significant difference (by one-way ANOVA, Tukey's comparison, $P < 0.05$). Con, control. Numbers in parentheses are neuromast numbers.

recover for up to 1 h after the AGs were washed out (data not shown). However, AG treatment did not alter Ca^{2+} fluxes of KCs (Fig. 6, *C* and *F*).

Addition of Ca^{2+} and Mg^{2+} neutralized inhibition by AGs. The Ca^{2+} level of NW (and recording medium) was 0.2 mM, which was close to the Ca^{2+} level of local tap water. To test if a high level of Ca^{2+} could neutralize inhibition by AGs, embryos were preincubated in AG medium with 0.2 (control) or 2 mM Ca^{2+} for 30 min and then measured with the SIET in recording medium without the AGs. Results showed that no significant decrease was found in neomycin groups (1~100 μM) with 2 mM Ca^{2+} (Fig. 6*B*). Similar effects were found for gentamicin treatments (Fig. 6*E*). These results showed that 2 mM Ca^{2+} completely neutralized the inhibition of up to 100 μM AGs, and partially neutralized the effect of 1,000 μM gentamicin. However, it did not neutralize the effect of 1,000 μM neomycin.

To further test the effects of Ca^{2+} and Mg^{2+} levels on AG inhibition, Ca^{2+} levels of AG media (100 μM neomycin or gentamicin) were adjusted to 0.2, 0.5, 1, 1.5, and 2 mM. Results showed that the effect of Ca^{2+} was concentration dependent (Fig. 7). Concentrations of <1.5 mM did not significantly affect inhibition by neomycin (Fig. 7*A*) or gentamicin (Fig. 7*B*). Mg^{2+} concentrations of 5 and 10 mM only partially neutralized inhibition by neomycin (Fig. 7*C*), whereas Mg^{2+} concentrations of >1 mM effectively neutralized the effect of gentamicin (Fig. 7*D*). Preincubating embryos with 2 mM Ca^{2+} (or Mg^{2+}) did not affect the Ca^{2+} influx of neuromasts (data not shown).

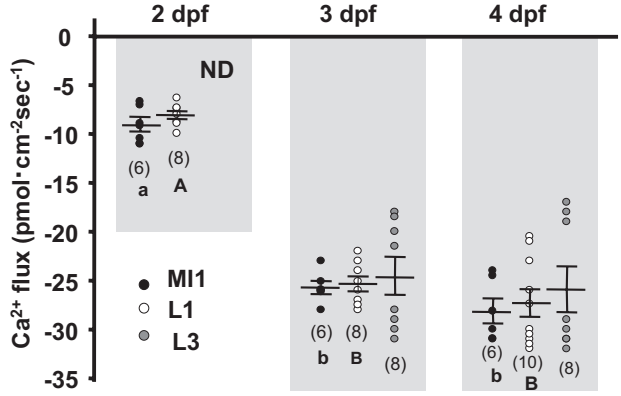

Fig. 5. Ca^{2+} influx of neuromasts during 2- to ~4-day postfertilization (dpf) embryonic development. MI1, L1, and L3 neuromasts of 2- to ~4-dpf zebrafish embryos were measured. The influx of the apical surface of L3 was not detectable (ND), and so it was not measured at 2 dpf. Data are presented as the means ± SE. [a,b(or A,B)]Significant difference of MI1 (or L1) neuromasts among different stages (by one-way ANOVA, Tukey's comparison, $P < 0.05$). Numbers in parentheses are neuromast numbers.

DISCUSSION

In this study, a noninvasive SIET was applied for the first time to investigate the activity of MET channels in neuromast hair cells of living zebrafish embryos. We used a Ca^{2+}-selective microelectrode driven by a motion system to deflect hair bundles of hair cells and simultaneously record Ca^{2+} fluxes at the apical surface of neuromasts. Inward Ca^{2+} fluxes were detected at stereocilia of L1~L3 neuromasts in 2- to ~4-dpf embryos, and the influx was blocked by MET channel blockers (BAPTA, La^{3+}, Gd^{3+}, and curare), suggesting that Ca^{2+} entry occurs via MET channels. AGs (10 μM neomycin or gentamicin) were found to effectively block Ca^{2+} influx within 10 min. Elevating the external Ca^{2+} or Mg^{2+} level neutralized inhibition by both neomycin and gentamicin. This study demonstrated and quantified MET channel-mediated

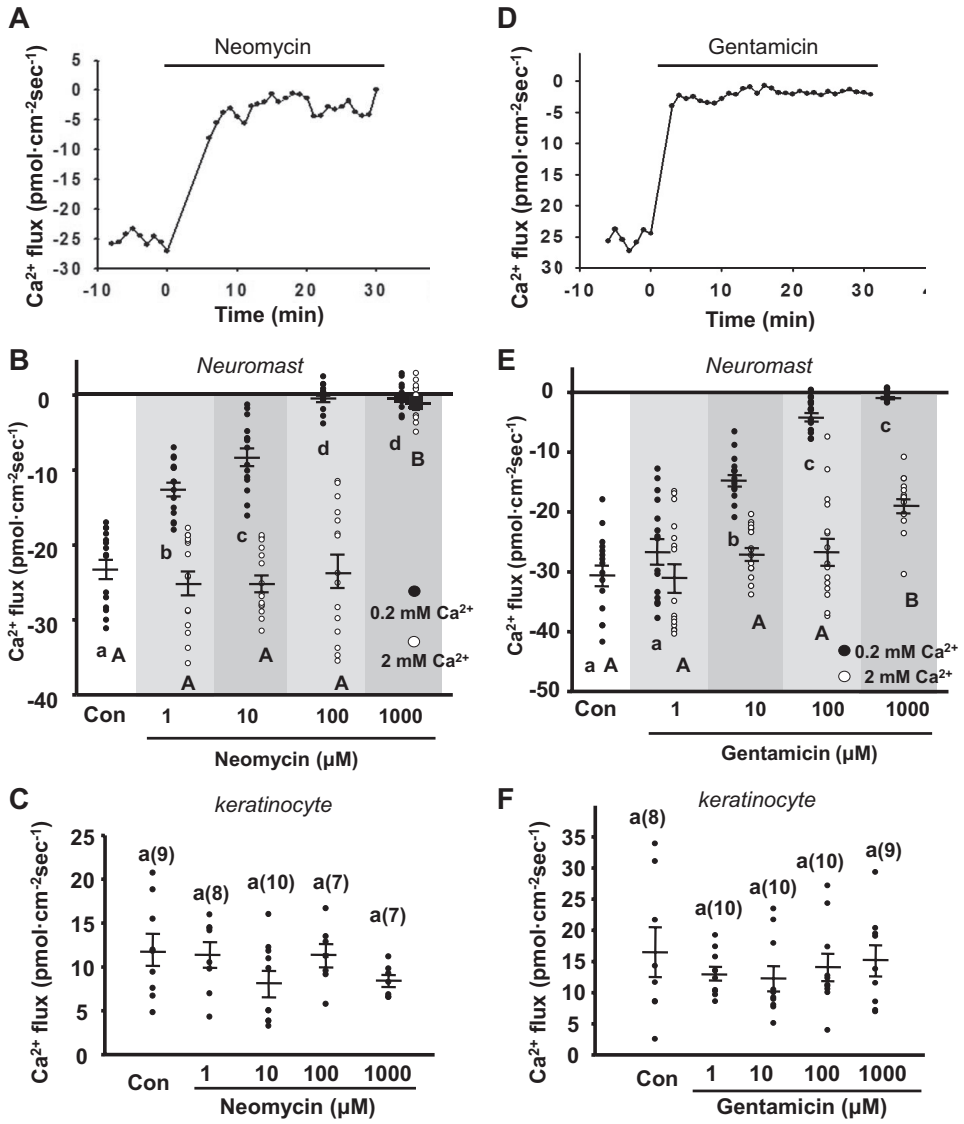

Fig. 6. Effect of neomycin on the Ca^{2+} influx of neuromasts. *A* and *D*: sequential recordings of Ca^{2+} influx of neuromasts before and after the addition of 10 μM neomycin or gentamicin. *B* and *E*: embryos were preincubated in normal water (black dots 0.2 mM Ca^{2+}) or high-Ca^{2+} normal water (white dots, 2 mM Ca^{2+}) with 1~1,000 μM neomycin (*B*) or gentamicin (*E*) for 30 min. Ca^{2+} influx was recorded in normal recording medium without neomycin or gentamicin. *C* and *F*: effects of neomycin (*C*) or gentamicin (*F*) on the Ca^{2+} flux of KC. Data are presented as the means ± SE. [a,b,c]Significant difference among the 0.2 mM Ca^{2+} groups; [A,B]Significant difference among the 2 mM Ca^{2+} and control groups (by one-way ANOVA, Tukey's comparison, $P < 0.05$). n = 15 neuromasts in *B* and *E*. *C* and *F*: numbers in parentheses are KC numbers.

Ca^{2+} influx at neuromasts and showed that the SIET is a suitable instrument for functionally assaying MET channels in living zebrafish embryos.

In previous studies, high-resolution intracellular Ca^{2+} images showed that MET channels are located at the tips of stereocilia in rat and bullfrog hair cells (5, 12, 35). A recent study found that MET channels were also located at kinocilia and mediated mechanosensitivity of 2-dpf zebrafish embryos (30). In this study, the Ca^{2+} influx was only detected at stereocilia and not at the tips of kinocilia (Fig. 2), suggesting that stereocilia are a major location of MET channels. However, we cannot exclude the possibility that MET channels are located in the basal region of kinocilia.

Previous studies showed that the appearance of ALL neuromasts followed a schedule from 34 to 72 hpf, and MI1 neuromasts we measured in this study appeared at 41 hpf (45). PLL neuromasts appear in the proper position by 2 dpf (29). In a recent study by Kindt and et al. (30), they found that MET channels were active in 2-dpf embryos. In this study, minor Ca^{2+} influxes were detected at MI1 and L1 neuromasts in 2-dpf zebrafish embryos (Fig. 5). At 2~3 dpf, afferent neurons begin to innervate hair cells (39), and embryos display an escape response triggered by water flow at 3 dpf (9). Taken together, results suggest that MET activity begins as early as 2 dpf. When more hair cells had matured, larger Ca^{2+} influx signals were detected in 3- and 4-dpf embryos (Fig. 5).

Several approaches have been used to analyze the function of MET channels. FM 1–43 was used as a marker of the viability of hair cells (8, 42, 50) and was also used as an indicator of functional MET channels, since it was found to enter hair cells through MET channels (16, 21, 38). However, FM 1–43 accumulation is a difficult way to quantify the activity of MET channels and cannot reveal real-time activity of MET channels. An electrophysiological approach, recording of the microphonic potential, is an alternative approach to determine the activity of MET channels (40). The microphonic potential represents the overall voltage response of hair cells, but the recorded potential cannot reveal the specific kind of ion activity involved in mechanotransduction.

Previous studies showed that MET channels have high Ca^{2+} permeability (4, 18, 41, 47) and used Ca^{2+} imaging to localize MET channels on hair cells (5, 12, 35). The highly Ca^{2+}-

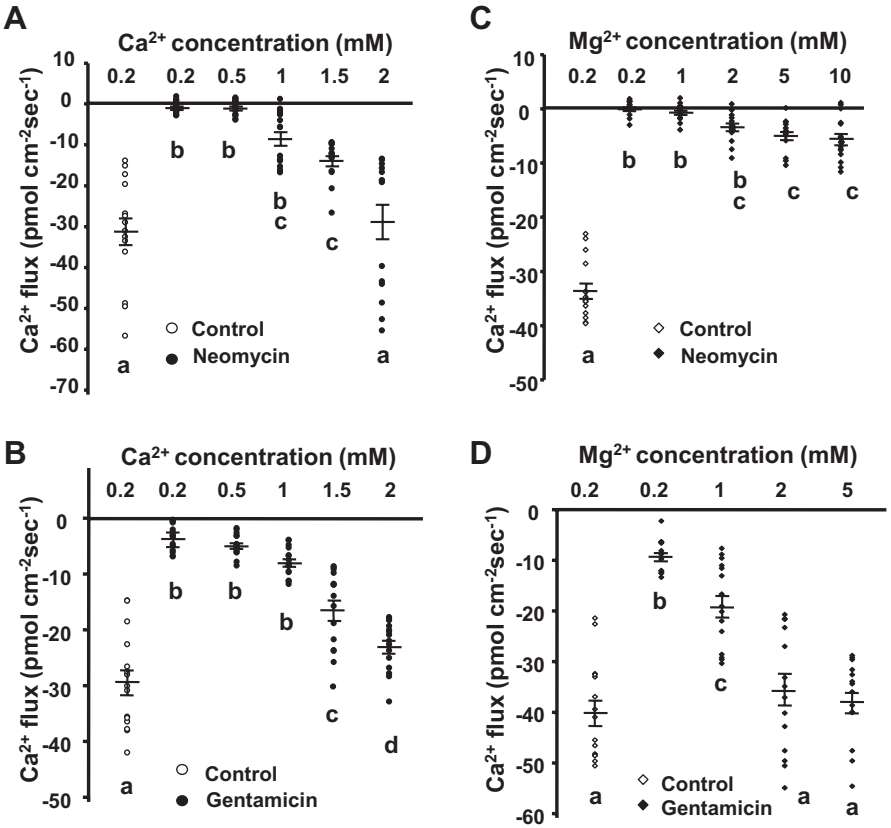

Fig. 7. Effects of external Ca^{2+} and Mg^{2+} levels on inhibition by 100 μM neomycin and gentamicin. *A–D*: embryos were preincubated in 100 μM neomycin (*A* and *C*) or gentamicin (*B* and *D*) media with different levels of Ca^{2+} (*A* and *B*) or Mg^{2+} (*C* and *D*) for 30 min. Ca^{2+} influx was recorded in normal recording medium. Data are presented as the means ± SE. ^{a,b,c,d}Significant difference (by one-way ANOVA, Tukey's comparison, $P < 0.05$); $n = 15$ neuromasts.

permeable transient receptor potential channel family was reported to be candidates for MET channels (10, 18). However, in the vertebrate inner ear, hair bundles are bathed in high-K^+ endolymph, and mechanotransduction is predominantly activated by K^+ entry through MET channels (18, 65). Nevertheless, K^+ influx was not detected at neuromasts of zebrafish in this study, showing that MET channels in a freshwater environment conduct Ca^{2+} instead of K^+ (Fig. 3A). This is reasonable, because K^+ levels in fresh water are supposedly much lower than intracellular K^+ levels. Moreover, we found that raising the external K^+ (5 mM) did not interfere with Ca^{2+} entry through MET channels (Fig. 3*B*). Therefore, the ion selectivity of neuromast MET channels and inner-ear MET channels might differ.

A number of studies found that AGs not only damaged human hair cells but also damaged zebrafish neuromast hair cells, suggesting that zebrafish embryos could be a model for ototoxin screening (7, 20, 43, 58). In zebrafish embryos, treatment with 25 μM neomycin or 50 μM gentamicin for 30 min caused around ~20% hair-cell death in neuromasts (8, 20, 50). Herein, we found that only 1 μM neomycin and 10 μM gentamicin could suppress the Ca^{2+} influx of neuromasts (Fig. 6, *B* and *E*) but caused no morphological changes, suggesting that the SIET is a very sensitive approach for detecting ototoxic effects. In addition, we found that 10 μM AGs quickly abolished Ca^{2+} influx (within 10 min), suggesting that AGs could block MET channels before triggering hair-cell death. In previous studies, an AG (DHS) was also suggested to block MET channels in isolated mouse hair cells (36, 41, 44, 46).

Even though endolymph Ca^{2+} levels are as low as ~0.02 mM in the rat and ~0.05 mM in the turtle (6, 11, 47), they seem to be crucial for hair cell function. Experiments in the mouse showed that neomycin provoked hair cell damage was suppressed by elevating Ca^{2+} or Mg^{2+} concentration and enhanced by withdrawing Ca^{2+} or Mg^{2+} (49). In zebrafish, increases in either extracellular Ca^{2+} or Mg^{2+} were also found to protect hair cells from AG-induced cell death and Ca^{2+}-free medium was found to cause hair-cell death (8). It has been shown that external Ca^{2+} enters MET channels and causes channel closure (adaptation) in turtle inner ears (11, 17, 47, 48). It has been suggested that elevating external Ca^{2+} might close MET channels and decrease DHS entry and DHS-induced channel blockage (36). Our results support this suggestion. However, we found that the relative potency of Ca^{2+} and Mg^{2+} differed: raising the Ca^{2+} level neutralized the blockade by both neomycin and gentamicin, whereas raising the Mg^{2+} level did not effectively neutralize the blockade by neomycin (Fig. 7). It is possible that Mg^{2+} only partially substitutes for the function of Ca^{2+} and is, thus, less effective.

The toxicity of AGs is affected by external divalent cations, and therefore, this factor should be considered in studies of hair cells. In previous studies on zebrafish, two different media (E3 medium and embryonic medium) were used for embryo incubation. The embryonic medium had higher Ca^{2+} (1 mM) and Mg^{2+} (1 mM) levels compared with E3 medium (0.33 mM Ca^{2+} and 0.33 mM Mg^{2+}) and our NW (0.2 mM Ca^{2+} and 0.2 mM Mg^{2+}). The NW we used mimicked local tap water for raising adult zebrafish, and this medium was used in all of our previous studies. Importantly, the Ca^{2+} level of endolymph of humans is extremely low (0.02 mM; Refs. 6, 63), and this might be a reason why hair cells are so sensitive to AGs.

GRANTS

This study was supported by National Science Council Grant NSC100-2311-B-038-001 and Taipei Medical University Grant TMU99-AE1-B18 (Taiwan, Republic of China; to J. L. Horng).

DISCLOSURES

No conflicts of interest, financial or otherwise, are declared by the author(s).

AUTHOR CONTRIBUTIONS

Author contributions: L.-Y.L., G.-Y.H., Y.-H.L., and J.-L.H. conception and design of research; L.-Y.L., W.P., W.-M.C., Y.-H.L., and J.-L.H. performed experiments; L.-Y.L., W.P., W.-M.C., Y.-H.L., and J.-L.H. analyzed data; L.-Y.L., G.-Y.H., and J.-L.H. interpreted results of experiments; L.-Y.L., W.P., W.-M.C., and J.-L.H. prepared figures; L.-Y.L., G.-Y.H., and J.-L.H. drafted manuscript; L.-Y.L. and J.-L.H. edited and revised manuscript; L.-Y.L. and J.-L.H. approved final version of manuscript.

REFERENCES

1. **Alharazneh A, Luk L, Huth M, Monfared A, Steyger PS, Cheng AG, Ricci AJ.** Functional hair cell mechanotransducer channels are required for aminoglycoside ototoxicity. *PLoS One* 6: e22347, 2011.
2. **Bashtanov ME, Goodyear RJ, Richardson GP, Russell IJ.** The mechanical properties of chick (*Gallus domesticus*) sensory hair bundles: relative contributions of structures sensitive to calcium chelation and subtilisin treatment. *J Physiol* 559: 287–299, 2004.
3. **Becvarovski Z, Michaelides EM, Kartush JM, Bojrab DI, LaRouere MJ.** Rapid elevation of gentamicin levels in the human labyrinth following intravenous administration. *Laryngoscope* 112: 1163–1165, 2002.
4. **Beurg M, Evans MG, Hackney CM, Fettiplace R.** A large-conductance calcium-selective mechanotransducer channel in mammalian cochlear hair cells. *J Neurosci* 26: 10992–11000, 2006.
5. **Beurg M, Fettiplace R, Nam JH, Ricci AJ.** Localization of inner hair cell mechanotransducer channels using high-speed calcium imaging. *Nat Neurosci* 12: 553–558, 2009.
6. **Bosher SK, Warren RL.** Very low calcium content of cochlear endolymph, an extracellular fluid. *Nature* 273: 377–378, 1978.
7. **Chiu LL, Cunningham LL, Raible DW, Rubel EW, Ou HC.** Using the zebrafish lateral line to screen for ototoxicity. *J Assoc Res Otolaryngol* 9: 178–190, 2008.
8. **Coffin AB, Reinhart KE, Owens KN, Raible DW, Rubel EW.** Extracellular divalent cations modulate aminoglycoside-induced hair cell death in the zebrafish lateral line. *Hear Res* 253: 42–51, 2009.
9. **Colwill RM, Creton R.** Imaging escape and avoidance behavior in zebrafish larvae. *Rev Neurosci* 22: 63–73, 2011.
10. **Corey DP.** What is the hair cell transduction channel? *J Physiol* 576: 23–28, 2006.
11. **Crawford AC, Evans MG, Fettiplace R.** The actions of calcium on the mechano-electrical transducer current of turtle hair cells. *J Physiol* 434: 369–398, 1991.
12. **Denk W, Holt JR, Shepherd GM, Corey DP.** Calcium imaging of single stereocilia in hair cells: localization of transduction channels at both ends of tip links. *Neuron* 15: 1311–1321, 1995.
13. **Donini A, Gaidhu MP, Strasberg DR, O'donnell MJ.** Changing salinity induces alterations in hemolymph ion concentrations and Na^+ and Cl^- transport kinetics of the anal papillae in the larval mosquito, Aedes aegypti. *J Exp Biol* 210: 983–992, 2007.
14. **Donini A, O'Donnell MJ.** Analysis of Na^+, Cl^-, K^+, H^+ and NH_4^+ concentration gradients adjacent to the surface of anal papillae of the mosquito Aedes aegypti: application of self-referencing ion-selective microelectrodes. *J Exp Biol* 208: 603–610, 2005.
15. **Dulon D, Hiel H, Aurousseau C, Erre JP, Aran JM.** Pharmacokinetics of gentamicin in the sensory hair cells of the organ of Corti: rapid uptake and long term persistence. *C R Acad Sci III* 316: 682–687, 1993.
16. **Ebert J, Fink S, Koitschev A, Walther P, Langer MG, Lehmann-Horn F.** Recovery of mechano-electrical transduction in rat cochlear hair bundles after postnatal destruction of the stereociliar cross-links. *Proc Biol Sci* 277: 2291–2299, 2010.
17. **Farris HE, Wells GB, Ricci AJ.** Steady-state adaptation of mechanotransduction modulates the resting potential of auditory hair cells, providing an assay for endolymph Ca^{2+}. *J Neurosci* 26: 12526–12536, 2006.
18. **Fettiplace R.** Defining features of the hair cell mechanoelectrical transducer channel. *Pflügers Arch* 458: 1115–1123, 2009.
19. **Fettiplace R, Ricci AJ, Hackney CM.** Clues to the cochlear amplifier from the turtle ear. *Trends Neurosci* 24: 169–175, 2001.
20. **Froehlicher M, Liedtke A, Groh KJ, Neuhauss SC, Segner H, Eggen RI.** Zebrafish (*Danio rerio*) neuromast: promising biological endpoint linking developmental and toxicological studies. *Aquat Toxicol (Amst)* 95: 307–319, 2009.
21. **Gale JE, Marcotti W, Kennedy HJ, Kros CJ, Richardson GP.** FM1–43 dye behaves as a permeant blocker of the hair-cell mechanotransducer channel. *J Neurosci* 21: 7013–7025, 2001.
22. **Garber SS, Messerli MA, Hubert M, Lewis R, Hammar K, Indyk E, Smith PJ.** Monitoring Cl^- movement in single cells exposed to hypotonic solution. *J Membr Biol* 203: 101–110, 2005.
23. **Ghysen A, Dambly-Chaudière C.** The lateral line microcosmos. *Genes Dev* 21: 2118–2130, 2007.
24. **Gleeson RA, Hammar K, Smith PJ.** Sustaining olfaction at low salinities: mapping ion flux associated with the olfactory sensilla of the blue crab Callinectes sapidus. *J Exp Biol* 203: 3145–3152, 2000.
25. **Horng JL, Lin LY, Huang CJ, Katoh F, Kaneko T, Hwang PP.** Knockdown of V-ATPase subunit A (*atp6v1a*) impairs acid secretion and ion balance in zebrafish (*Danio rerio*). *Am J Physiol Regul Integr Comp Physiol* 292: R2068–R2076, 2007.
26. **Horng JL, Lin LY, Hwang PP.** Functional regulation of H^+-ATPase-rich cells in zebrafish embryos acclimated to an acidic environment. *Am J Physiol Cell Physiol* 296: C682–C692, 2009.
27. **Huth ME, Ricci AJ, Cheng AG.** Mechanisms of aminoglycoside ototoxicity and targets of hair cell protection. *Int J Otolaryngol* 2011: 937861, 2011.
28. **Hwang PP, Perry S.** Ionic and acid-base regulation. In: *Zebrafish. Fish Physiology Volume*, edited by Perry S, Ekker M, Farrell AP, Brauner CJ. New York: Academic, 2010, p. 311–314.
29. **Kimmel CB, Ballard WW, Kimmel SR, Ullmann B, Schilling TF.** Stages of embryonic development of the zebrafish. *Dev Dyn* 203: 253–310, 1995.
30. **Kindt KS, Finch G, Nicolson T.** Kinocilia mediate mechanosensitivity in developing zebrafish hair cells. *Dev Cell* 23: 329–41, 2012.
31. **Kreitzer MA, Collis LP, Molina AJ, Smith PJ, Malchow RP.** Modulation of extracellular proton fluxes from retinal horizontal cells of the catfish by depolarization and glutamate. *J Gen Physiol* 130: 169–182, 2007.
32. **Kroese AB, Das A, Hudspeth AJ.** Blockage of the transduction channels of hair cells in the bullfrog's sacculus by aminoglycoside antibiotics. *Hear Res* 37: 203–217, 1989.
33. **Li H, Steyger PS.** Synergistic ototoxicity due to noise exposure and aminoglycoside antibiotics. *Noise Health* 11: 26–32, 2009.
34. **Lin LY, Horng JL, Kunkel JG, Hwang PP.** Proton pump-rich cell secretes acid in skin of zebrafish larvae. *Am J Physiol Cell Physiol* 290: C371–C378, 2006.
35. **Lumpkin EA, Hudspeth AJ.** Detection of Ca^{2+} entry through mechanosensitive channels localizes the site of mechanoelectrical transduction in hair cells. *Proc Natl Acad Sci USA* 92: 10297–10301, 1995.
36. **Marcotti W, van Netten SM, Kros CJ.** The aminoglycoside antibiotic dihydrostreptomycin rapidly enters mouse outer hair cells through the mechano-electrical transducer channels. *J Physiol* 567: 505–521, 2005.
37. **Messerli MA, Smith PJ, Lewis RC, Robinson KR.** Chloride fluxes in lily pollen tubes: a critical reevaluation. *Plant J* 40: 799–812, 2004.
38. **Meyers JR, MacDonald RB, Duggan A, Lenzi D, Standaert DG, Corwin JT, Corey DP.** Lighting up the senses: FM1–43 loading of sensory cells through nonselective ion channels. *J Neurosci* 23, 4054–4065, 2003.
39. **Nagiel A, Andor-Ardó D, Hudspeth AJ.** Specificity of afferent synapses onto plane-polarized hair cells in the posterior lateral line of the zebrafish. *J Neurosci* 28: 8442–8453, 2008.
40. **Nicolson T, Rusch A, Friedrich RW, Granato M, Ruppersberg JP, Nusslein-Volhard C.** Genetic analysis of vertebrate sensory hair cell mechanosensation: the zebrafish circler mutants. *Neuron* 20: 271–283, 1998.
41. **Ohmori H.** Mechano-electrical transduction currents in isolated vestibular hair cells of the chick. *J Physiol* 359: 189–217, 1985.
42. **Ou HC, Raible DW, Rubel EW.** Cisplatin-induced hair cell loss in zebrafish (*Danio rerio*) lateral line. *Hear Res* 233: 46–53, 2007.
43. **Ou HC, Santos F, Raible DW, Simon JA, Rubel EW.** Drug screening for hearing loss: using the zebrafish lateral line to screen for drugs that prevent and cause hearing loss. *Drug Discov Today* 15: 265–271, 2010.

44. **Preyer S, Hemmert W, Zenner HP, Gummer AW.** Abolition of the receptor potential response of isolated mammalian outer hair cells by hair-bundle treatment with elastase: a test of the tip-link hypothesis. *Hear Res* 89: 187–93, 1995.
45. **Raible DW, Kruse GJ.** Organization of the lateral line system in embryonic zebrafish. *J Comp Neurol* 421: 189–198, 2000.
46. **Ricci A.** Differences in mechano-transducer channel kinetics underlie tonotopic distribution of fast adaptation in auditory hair cells. *J Neurophysiol* 87: 1738–1748, 2002.
47. **Ricci AJ, Fettiplace R.** Calcium permeation of the turtle hair cell mechanotransducer channel and its relation to the composition of endolymph. *J Physiol* 506: 159–173, 1998.
48. **Ricci AJ, Kennedy HJ, Crawford AC, Fettiplace R.** The transduction channel filter in auditory hair cells. *J Neurosci* 25: 7831–7839, 2005.
49. **Richardson GP, Russell IJ.** Cochlear cultures as a model system for studying aminoglycoside induced ototoxicity. *Hear Res* 53: 293–311, 1991.
50. **Santos F, MacDonald G, Rubel EW, Raible DW.** Lateral line hair cell maturation is a determinant of aminoglycoside susceptibility in zebrafish (*Danio rerio*). *Hear Res* 213: 25–33, 2006.
51. **Schwander M, Kachar B, Müller U.** The cell biology of hearing. *J Cell Biol* 190: 9–20, 2010.
52. **Seligmann H, Podoshin L, Ben-David J, Fradis M, Goldsher M.** Drug-induced tinnitus and other hearing disorders. *Drug Saf* 14: 198–212, 1996.
53. **Shen WP, Horng JL, Lin LY.** Functional plasticity of mitochondrion-rich cells in the skin of euryhaline medaka larvae (*Oryzias latipes*) subjected to salinity changes. *Am J Physiol Regul Integr Comp Physiol* 300: R858–R868, 2011.
54. **Shih TH, Horng JL, Liu ST, Hwang PP, Lin LY.** Rhcg1 and NHE3b are involved in ammonium-dependent sodium uptake by zebrafish larvae acclimated to low-sodium water. *Am J Physiol Regul Integr Comp Physiol* 302: R84–R93, 2012.
55. **Shih TH, Horng JL, Hwang PP, Lin LY.** Ammonia secretion in skin of zebrafish larvae (*Danio rerio*). *Am J Physiol Cell Physiol* 295: C1625–C1632, 2008.
56. **Smith PJ, Hammar K, Porterfield DM, Sanger RH, Trimarchi JR.** Self-referencing, non-invasive, ion selective electrode for single cell detection of trans-plasma membrane calcium flux. *Microsc Res Tech* 46: 398–417, 1999.
57. **Sun J, Chen S, Dai S, Wang R, Li N, Shen X, Zhou X, Lu C, Zheng X, Hu Z, Zhang Z, Song J, Xu Y.** NaCl-induced alternations of cellular and tissue ion fluxes in roots of salt-resistant and salt-sensitive poplar species. *Plant Physiol* 149: 1141–1153, 2009.
58. **Ton C, Parng C.** The use of zebrafish for assessing ototoxic and otoprotective agents. *Hear Res* 208: 79–88, 2005.
59. **Tran Ba Huy P, Bernard P, Schacht J.** Kinetics of gentamicin uptake and release in the rat: comparison of inner ear tissues and fluids with other organs. *J Clin Invest* 77: 1492–1500, 1986.
60. **Waguespack JR, Ricci AJ.** Aminoglycoside ototoxicity: permeant drugs cause permanent hair cell loss. *J Physiol* 567: 359–360, 2005.
61. **Wang Q, Steyger PS.** Trafficking of systemic fluorescent gentamicin into the cochlea and hair cells. *J Assoc Res Otolaryngol* 10: 205–219, 2009.
62. **Warchol ME.** Cellular mechanisms of aminoglycoside ototoxicity. *Curr Opin Otolaryngol Head Neck Surg* 18: 454–458, 2010.
63. **Wangemann P.** Cochlear homeostasis and homeostatic disorders. In: *Handbook of Auditory Research. Auditory Trauma and Protection*, edited by Schacht J, Popper AN, Fay RR. New York: Springer, 2008, p. 49–100.
64. **Wu SC, Horng JL, Liu ST, Hwang PP, Wen ZH, Lin CS, Lin LY.** Ammonium-dependent sodium uptake in mitochondrion-rich cells of medaka (*Oryzias latipes*) larvae. *Am J Physiol Cell Physiol* 298: C237–C250, 2010.
65. **Zdebik AA, Wangemann P, Jentsch TJ.** Potassium ion movement in the inner ear: insights from genetic disease and mouse models. *Physiology (Bethesda)* 24: 307–316, 2009.